

An Adaptive Parallel Arc-Length Method

H.M. Verhelst^{a,b,*}, J.H. Den Besten^a, M. Möller^b

^a*Delft University of Technology, Department of Maritime and Transport Technology, Mekelweg 2, Delft 2628 CD, The Netherlands*

^b*Delft University of Technology, Department of Applied Mathematics, Van Mourik Broekmanweg 6, Delft 2628 XE, The Netherlands*

Abstract

Parallel computing is omnipresent in today's scientific computer landscape, starting at multicore processors in desktop computers up to massively parallel clusters. While domain decomposition methods have a long tradition in computational mechanics to decompose spatial problems into multiple subproblems that can be solved in parallel, advancing solution schemes for dynamics or quasi-statics are inherently serial processes. For quasi-static simulations, however, there is no accumulating 'time' discretization error, hence an alternative approach is required. In this paper, we present an Adaptive Parallel Arc-Length Method (APALM). By using a domain parametrization of the arc-length instead of time, the multi-level error for the arc-length parametrization is formed by the load parameter and the solution norm. By applying local refinements in the arc-length parameter, the APALM refines solutions where the non-linearity in the load-response space is maximal. The concept is easily extended for bifurcation problems. The performance of the method is demonstrated using isogeometric Kirchhoff-Love shells on problems with snap-through and pitch-fork instabilities. It can be concluded that the adaptivity of the method works as expected and that a relatively coarse approximation of the serial initialization can already be used to produce a good approximation in parallel.

Keywords: Arc-length methods, Parallelization, isogeometric analysis, Kirchhoff-Love shell, Post-buckling

1. Introduction

Over the last decades, computational power has increased exponentially. In the last year, most improvements are thanks to an increasing number of threads per processing unit rather than an increase in the single-thread performance [1]. The trend of increasing logical cores with a stagnating single thread performance calls for parallelization of existing codes to improve the computational efficiency, amongst which numerical algorithms in computational mechanics. In the field of computational mechanics, parallelization in the spatial domain is common practice by using shared-memory assembly routines or distributed-memory parallelization using domain decomposition of meshes. Parallelization can also be achieved in linear solvers or in the temporal domain using parallel-in-time solvers [2] in case of dynamic analyses or using parallel continuation for quasi-static or continuation problems - the latter two being sequential by nature.

For quasi-static problems, continuation methods can be used when the solution of an equation or a system of equa-

*Corresponding Author.

Email addresses: h.m.verhelst@tudelft.nl (H.M. Verhelst), henk.denbesten@tudelft.nl (J.H. Den Besten), m.moller@tudelft.nl (M. Möller)

tions is desired, given varying parameters of the system. Such methods, typically referred to as Arc-Length Methods (ALMs), are widely used for (but not limited to) the analysis of the stability of structures. The Riks and Crisfield methods [3, 4] are commonly used and in combination with bifurcation algorithms [5], whereas ALMs provide a valuable tool in the analysis of the collapse and post-buckling behaviour of structures. Recent developments for ALMs include a new displacement-controlled formulation [6], an improved predictor scheme [7] and automatic exploration techniques [8, 9]. Alike time-stepping methods, ALMs are sequential by nature, meaning that the solution in a point is obtained from the solution in a point obtained previously.

Amongst many parallel time-integration schemes, Parareal is a parallel time-integration method proposed by [10] and works with a two-level parallel correction scheme of time intervals. The method starts from a series of solutions obtained in serial with a large time-step, after which each sub-interval is computed with a finer time-step such that a new solution is found at the end-point of the time interval. A multi-level extension of Parareal is proposed in [11] and is referred to as Multi-Grid Reduced In Time (MGRIT). This method is similar to Parareal but applies the two-level approach recursively. As a consequence, multi-grid-like cycles can be used to correct previously computed sub-intervals. This method has not only been applied to dynamic problems, but also to the training of neural networks [12] and [13]. Alternative methods for parallel time integration methods are reviewed in the work of [2].

Compared to temporal parallelization methods, parallelization of ALMs has received less attention in the academic community. As ALMs are typically used for explorations of solutions across branches, parallel evaluation of branches can be performed as soon as the starting point (and tangent) of each branch is known. The number of branches related to a problem, however, depends typically on the problem that is solved, hence parallel scalability of ALMs over branches is not guaranteed. A parallelization within a branch is enabled by the Parallel Adaptive Method for Pseudo-Arclength Continuation (PAMPAC) [14]. This method works with multiple predictors (with different step sizes) and consequently correctors to select an optimal step size; which can be performed in parallel. The PAMPAC method focusses on selecting a maximal step size for the ALM for which the method does not converge.

In this paper, a parallelization of the arc-length method is presented, which is independent of the physical nature of the underlying problem. That is, the method is developed such that the parallelization can be performed within the branches. In addition to parallelization, the presented arc-length scheme also provides inherent adaptivity, therefore the method is referred to as the Adaptive Parallel Arc-Length Method (APALM). The working principle of the APALM is based on a multi-level approach - inspired by MGRIT methods - where a coarse serial approximation of the solution space is refined in parallel until a measure of convergence is achieved. Contrary to the PAMPAC, the present method does not maximize the step size for convergence of the ALM iterations, but instead the parallelization is based on convergence of the solution on sub-intervals. Without loss of generality, the method is developed given a constraint equation for the arc-length method; thus generalized for Riks and Crisfield methods, amongst other methods available.

The outline of this paper is as follows. Section 2 provides a background on arc-length methods. In section 3 the parallelization of arc-length methods is presented, referred to as the APALM. Thereafter section 4 provides algorithms for non-intrusive implementation of the APALM, given an implementation of an existing ALM. Finally, section 5 and section 6 provide results and conclusions.

2. Arc-Length methods

In this section, the concept of arc-length methods is presented for the sake of completeness. For a detailed overview, one can consult references [3, 4, 15, 16]. Let $\mathbf{G}(\mathbf{u}, \lambda) = \mathbf{0}$ be a non-linear system of equations to be solved, with \mathbf{u} the solution to the system of equations given a parameter λ . For structural analyses, \mathbf{u} is typically a vector containing discrete displacements of the degrees of freedom and λ is a factor scaling the magnitude of an applied load P , i.e.

$$\mathbf{G}(\mathbf{u}, \lambda) = \mathbf{N}(\mathbf{u}) - \lambda \mathbf{P}, \quad (1)$$

where $\mathbf{N}(\mathbf{u})$ is a vector of internal forces, depending on the deformation \mathbf{u} . For incremental analyses, i.e. quasi-static analyses, a series of solutions $\mathbf{w}_i = (\mathbf{u}_i, \lambda_i)$ is obtained by computing increments $\Delta \mathbf{w}_i = (\Delta \mathbf{u}_i, \Delta \lambda_i)$ such that $\mathbf{w}_{i+1} = \mathbf{w}_i + \Delta \mathbf{w}_i$ and equation (1) is satisfied for \mathbf{w}_{i+1} . These solutions can be obtained by Newton iterations, i) fixing λ and finding \mathbf{u} (*load control*), ii) fixing some degrees of freedom in \mathbf{u} and finding all \mathbf{u} and λ (*displacement control*) or iii) constraining λ and \mathbf{u} and solving for both (*arc-length control*), see figure 1. In case of arc-length control, the increment $\Delta \mathbf{w}$ is measured by an increment length $d(\Delta \mathbf{w})$

$$d(\Delta \mathbf{w}) = \Delta \mathbf{u}^\top \Delta \mathbf{u} + \Psi^2 \Delta \lambda^2 \mathbf{P}^\top \mathbf{P}, \quad (2)$$

where Ψ is a scaling parameter given in [17, 18]. The increment $\Delta \mathbf{w}$ is constrained by the arc-length $\Delta \ell$ in the constraint equation

$$f(\Delta \mathbf{w}) = d(\Delta \mathbf{w}) - \Delta \ell = 0. \quad (3)$$

Since $\mathbf{G}(\mathbf{u}, \lambda)$ is non-linear, the increment $\Delta \mathbf{w}_i$ is obtained iteratively, i.e. $\Delta \mathbf{w}_{i,k+1} = \Delta \mathbf{w}_{i,k} + \delta \mathbf{w}_i$ with iteration count k . The constraint equation is solved together with equation (1) in every iteration, yielding the Riks and Crisfield methods [3, 4]

$$f(\Delta \mathbf{w}_{i,k}, \Delta l) = \Delta \mathbf{u}_{i,0}^\top \Delta \mathbf{u}_{i,k} + \Psi^2 \Delta \lambda_{i,0} \Delta \lambda_{i,k} \mathbf{P}^\top \mathbf{P} - \Delta \ell^2 = 0, \quad \text{Riks}, \quad (4)$$

$$f(\Delta \mathbf{w}_{i,k}, \Delta l) = \Delta \mathbf{u}_{i,k}^\top \Delta \mathbf{u}_{i,k} + \Psi^2 \Delta \lambda_{i,k} \Delta \lambda_{i,k} \mathbf{P}^\top \mathbf{P} - \Delta \ell^2 = 0, \quad \text{Crisfield}, \quad (5)$$

where $\Delta \mathbf{w}_0$ is the increment in the first iteration. The Crisfield method generally performs well with sharp snap-backs, but has the disadvantage that the constraint equation has two intersections with the path formed by equation (1). Hence a root has to be selected, which is elaborated in the works [4, 15]. When multiple intersections are found, complex roots are found [19] which can be resolved using one of the methods proposed in [20, 21].

3. Adaptive Parallel Arc-Length Method

In this section, our new approach, the APALM, is presented. Firstly, the method is conceptualized along with some illustrative figures (section 3.1). Secondly, details are provided on the curve parameterization and the measurement of

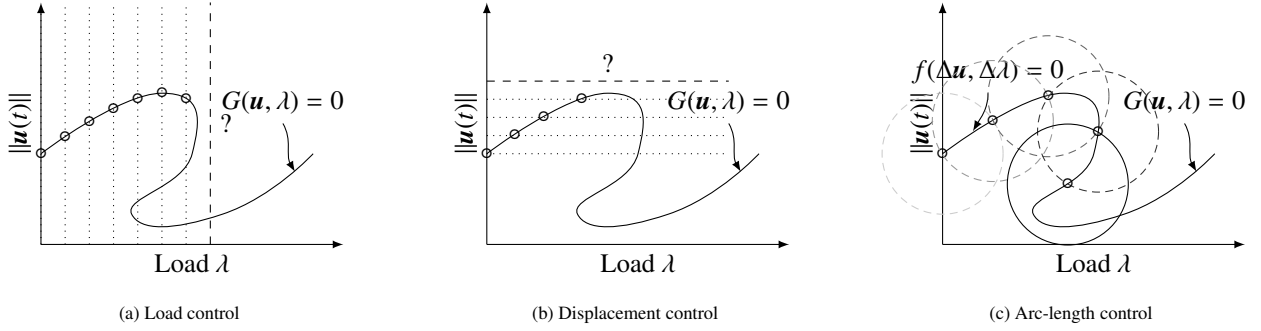


Figure 1: Load (left), displacement (middle) and arc-length control (right) for structural analysis problems. The question mark (?) indicates the iteration where load and displacement control encounter a limit point. In these situations, the next obtained point is typically difficult to find.

errors (section 3.2). Lastly, section 3.3 presents (re-)parameterization methods for the solution curve. These parameterizations will be essential in the data structure of the APALM. It should be noted that the method described in this section is presented only for one continuation parameter λ .

3.1. Concept

Learning from parallel-in-time methods like Parareal or MGRIT, parallelization with in the APALM is achieved from a subdivision of the *curve length domain*. Contrary to MGRIT and Parareal, where the temporal domain $t \in [T_0, T_1]$ is fixed, the APALM will work with a changing *curve length domain* $s \in [S_0, S_1]$ depending on the length of the traversed path, with an underlying fixed parametric domain with parametric coordinate $\xi \in [0, 1]$. The APALM is initialized with an initial coarse grid approximation, in which the parametric and the curve length domains are subdivided into sub-domains $\xi \in [\xi_i, \xi_{i+1}]$ and $s \in [s_i, s_{i+1}]$, respectively, as illustrated in figure 2.

In the initialization phase of the APALM the first subdivision into sub-intervals is made (see figure 2a). Here, the sizes of the sub-intervals $s \in [s_i^\ell, s_{i+1}^\ell]$ are determined based on the distance measure that is used by the corresponding ALM, see equation (2). Note that the superscript ℓ denotes the ℓ^{th} level. Based on the initial curve-length domain $s \in [0, S]$, where S is the total length of the initial curve, and the corresponding sub-intervals, the curve-length domain can be mapped accordingly onto a parametric domain, see section 4 for more details.

Having an initialized computational domain, the number of sub-intervals determines the degree of parallelization. On any sub-interval $[s_i^\ell, s_{i+1}^\ell]$ data at the start-point and end-point is known, which can be used to initiate an arc-length method to re-compute the sub-interval with N increments, i.e. with an arc-length of $\Delta L_i^{\ell+1} = \Delta L_i^\ell / N$ (see figure 2b).

After sub-interval $[s_i^{\ell+1}, s_{i+1}^{\ell+1}]$ has been finished, the distance of the end-point of the sub-interval can be compared to the previously known solution at s_{i+1}^ℓ , which is called *parallel verification of intervals* in figure 2c. Since the sub-interval is traversed in N increments with length $\Delta s_i^0 / N$, the triangle inequality with the arc-length measure implies that there must be a distance greater than or equal to zero between the newly found end-point and the reference end-point. The more

‘curved’ the domain in-between, the larger this distance. Based on an error measure (see section 3.2), intervals with a relatively large deviation between the coarse-level arc-length and the fine-level arc-length are to be marked for ‘refinement’.

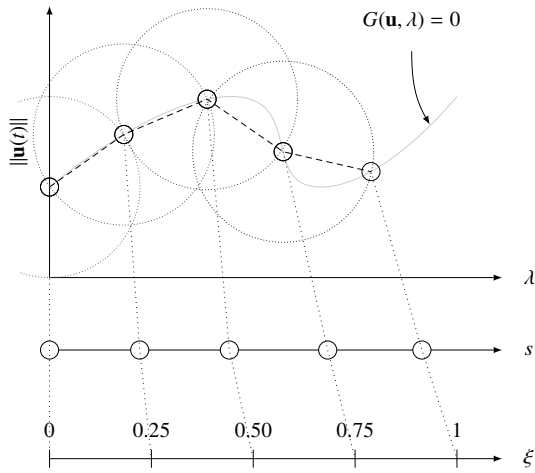
Lastly, the intervals with a too large deviation in the newly computed curve length need to be reparameterized (see section 3.3). This is, the total curve-length parameterization is elongated exactly by the distance between the newly computed end-point and the previously known point. By this means, the reference interval is subdivided to $N + 1$ sub-intervals and the data corresponding to the N newly computed point is stored. For sub-intervals that have an error below the tolerance, only $N - 1$ points are stored as reference and no reparameterization takes place. The process is sketched in figure 2d. After reparameterization, the marked interval can be re-computed and the process can be repeated from figure 2b onwards.

Remark 1 (Difference with parallel-in-time methods). *As mentioned, the multi-level approach that is employed in this method is adopted from the idea of parallel-in-time methods. However, the fundamental difference between time integration and continuation comes from the fact that time integration methods typically compute the solution on the next time step with a certain time integration error $O(\Delta t^p)$. Parallel-in-time methods rely on this time integration error, to mark solution intervals as converged or not and additionally updated solutions contain smaller time integration errors, and therefore sub-intervals need to be recomputed as soon as solutions previously in time have been updated.*

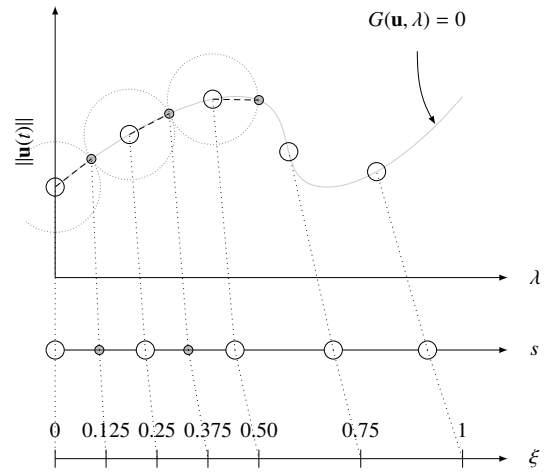
For arc-length methods, Newton’s method is applied on a system of equations that solves the arc-length constraint equation together with the discretized system $\mathbf{G}(\mathbf{u}, \lambda) = \mathbf{0}$. Therefore, the error of the solution that is found after an arc-length increment is independent of the arc-length increment size, but solely depends on the convergence tolerance of Newton’s method. Therefore, the end-point of an interval does not have to be updated, neither do intervals after the updated be recomputed.

3.2. Error measures

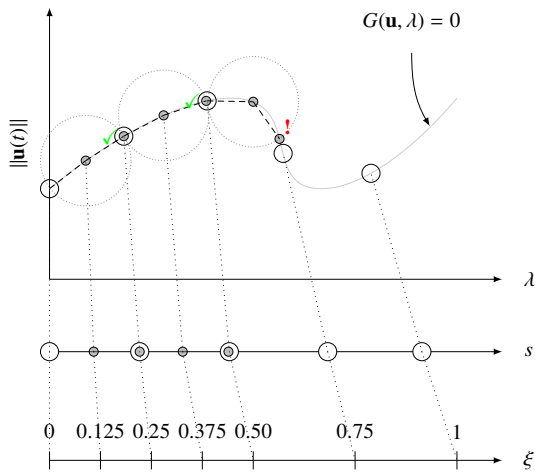
Refinement of computed sub-intervals is depending on the distances between the points in the original (coarse) interval and the newly obtained solutions in this sub-interval. Here, we present error measures that can be used to mark an interval $[s_i^\ell, s_{i+1}^\ell]$ based on the obtained solutions $\{s_k^{\ell+1}\}_{k=0, \dots, N}$ at the finer level. Figure 3 presents two possible situations; a nearly straight interval that would not be marked for refinement, and a curved interval that would be marked for refinement. Here, the interval is considered ‘curved’ in the discrete solution space if the hyperdimensional path between two solutions differs from the hyperplane between these solutions. The errors that determine the marking of an interval for refinement are illustrated in figure 3b and can be interpreted as follows: ΔL is the original arc-length between two coarse solutions, $\Delta L'$ is the newly obtained length between two coarse solutions, the *lower distance* $\overline{\Delta L}$ is the distance between the start of the interval and the last solution at the fine level and δL is the distance between the last obtained solution on the fine level and the final point on the coarse level. Using these distances, the *total error* (ε), the



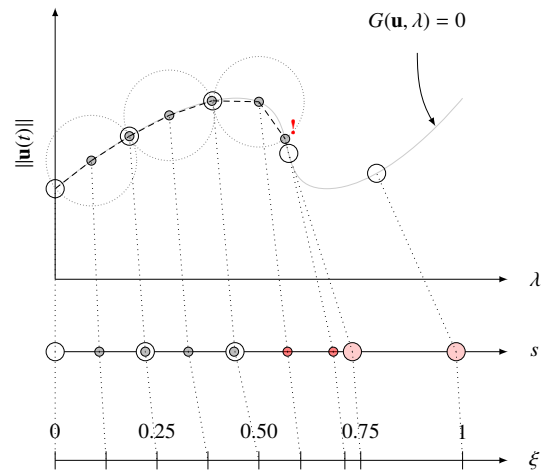
(a) **Initialization based on computed reference solutions.** Without losing generality, the solutions are separated with a fixed distance Δs . Given their distances, an initial estimation of the *curve length* s can be produced, which can be mapped on the *parametric domain* ξ .



(b) **Parallel computation of intervals.** On each interval, a finer estimate can be performed by splitting the interval in n sub-intervals ($n = 2$ here).

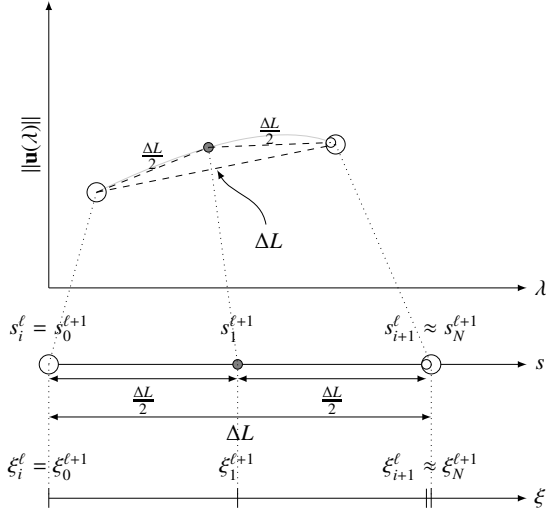


(c) **Parallel verification of intervals.** When the last sub-interval is computed, the solution is verified with the next known reference solution (here the solutions following from the initial simulations). When the distance is sufficiently small, the segment can be marked converged and the in between solutions on the interval can be written.

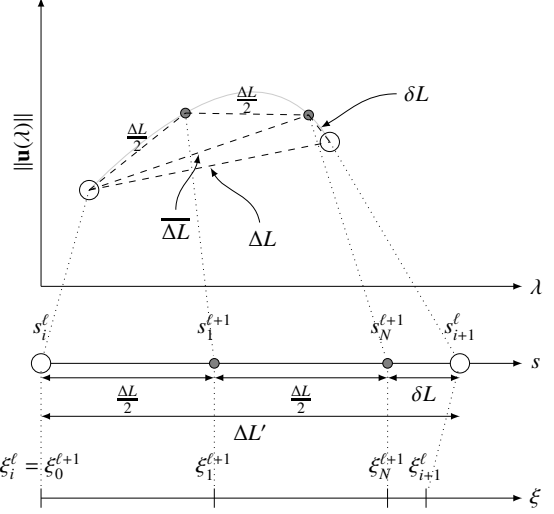


(d) **Curve-length reparameterization.** For sub-intervals where the length deviates too much from the previous length, i.e. where the distance between the last computed point and the reference is too large, all solutions of the sub-interval are added to the parameterization and the known data points ahead of the newly computed points are shifted in the curve parametric coordinates.

Figure 2: Concept of the APALM. The large open circles represent *reference solutions* from a previously computed level. The small solid circles represent *new data* on the interval between two reference solutions, computed by the arc-length method (here the large dashed circle). The black dashed line indicates the curve estimation of which the sum is equal to the total curve length.



(a) Nearly straight interval where the small white dot is sufficiently close to the coarse reference. In this case, the solution of the second increment is not added to the parameterization.



(b) Curved interval where the solution of the second increment is ΔL_u away from the coarse reference. In this case, the distance between the coarse reference points δL is smaller than the actually traversed distance $\Delta L'$.

Figure 3: Error measures on a nearly straight interval (a) and a curved interval (b). For the nearly straight interval, the distance δL (see b) is sufficiently small, whereas for the curved interval it is too big. The measures ΔL and $\Delta L'$, $\overline{\Delta L}$, δL are, respectively, the coarse arc-length, the fine arc-length, the lower distance and the absolute error.

lower error (ε_l) and the upper error (ε_u) can be defined:

$$\varepsilon = (\Delta L' - \Delta L)/\Delta L, \quad \text{total error,} \quad (6)$$

$$\varepsilon_l = (\Delta L - \overline{\Delta L})/\Delta L, \quad \text{lower error,} \quad (7)$$

$$\varepsilon_u = (\varepsilon - \varepsilon_l)/\Delta L, \quad \text{upper error.} \quad (8)$$

Here, the total error is the total difference between the coarse and fine intervals, the lower error is the contribution of the first N sub-intervals and the upper error is the contribution of δL to the total error. Depending on these errors and specified tolerances, refinement rules can be set-up; in particular:

$$\text{Refine the first } N \text{ intervals} \iff \varepsilon_l > \text{TOL}_l, \quad (9)$$

$$\text{Refine the last interval} \iff \varepsilon_u > \text{TOL}_u. \quad (10)$$

3.3. Curve (re-)parameterization

As indicated in figure 2, the concept of the APALM is supported by the parameterization of the solutions of $G(\mathbf{u}, \lambda) = \mathbf{0}$ by parameterizing the curve length using the increment length $d(\Delta \mathbf{w})$ embedded in the arc-length method. As illustrated in figure 2, the APALM maps solutions \mathbf{w} to a point on the curve-length domain $[0, S]$ and points on the curve length domain are mapped on a parametric domain $[0, 1]$.

Provided a series of solutions from the initialization phase $\{\mathbf{w}_i^0\}_{i=0, \dots, I}$, with I denoting the total number of initial points, and defining solution intervals by $\Delta \mathbf{w}_i^\ell = \mathbf{w}_{i+1}^\ell - \mathbf{w}_i^\ell$, each solution \mathbf{w}_i^0 can recursively be assigned to the curve-

length and parametric domains by

$$s_{i+1}^0 = s_i^0 + d(\Delta \mathbf{w}_i^0), \quad i = 1, \dots, I-1, \quad s_0 = 0, \quad (11)$$

$$\xi_i^0 = \frac{s_i}{s_I}, \quad i = 0, \dots, I, \quad (12)$$

where the superscript 0 represents the 0th level. In addition, equation (11) guarantees that $S = s_I$ marks the total length of the curve that has been traversed, measured by the distance between each solution. Given the curve-length coordinates of each point as an increasing sequence, the parametric domain can simply be obtained by scaling the domain back to $[0, 1]$, see equation (12). In the following, two ways of adding solutions to the parameterization are defined: i) interior insertion, and ii) full insertion and stretching. The operations are defined given a parent interval $[s_i^\ell, s_{i+1}^\ell)$ in which a set of new solutions $\{s_k^{\ell+1}\}_{k=0, \dots, N}$, where $s_0^{\ell+1} = s_i^\ell$, is computed, with N the total number of points in the interval, see figure 4a.

Firstly, the interior insertion operation inserts solutions *within* the sub-interval, see figure 4b, and is later used for intervals where the error small. The idea behind this operation is that the solutions $\{s_k^{\ell+1}\}_{k=1, \dots, N-1}$ between s_i^ℓ and s_{i+1}^ℓ are inserted and that the solution $s_N^{\ell+1}$ is not added to the map. In case of the interior insertion, the points $s_k^{\ell+1}$ and their parametric coordinates $\xi_k^{\ell+1}$ are added by:

$$s_{k+1}^{\ell+1} = s_k^{\ell+1} + d(\Delta \mathbf{w}_k^{\ell+1}), \quad k = 0, \dots, N-2, \quad s_0^{\ell+1} = s_i^\ell, \quad s_N^{\ell+1} = s_{i+1}^\ell, \quad (13)$$

$$\xi_{k+1}^{\ell+1} = \xi_k^{\ell+1} + (\xi_{i+1}^\ell - \xi_i^\ell) \frac{s_{k+1}^{\ell+1} - s_k^{\ell+1}}{s_{i+1}^\ell - s_i^\ell}, \quad j = 0, \dots, N-2. \quad (14)$$

Note that $\mathbf{w}_k^{\ell+1}$ denotes the k^{th} on level $\ell + 1$ on the computed sub-interval, here $[s_i^\ell, s_{i+1}^\ell]$.

The full insertion and stretching operation inserts the solutions of the sub-interval including its end-point, and also stretches the curve parameterization (see figure 4c), which is later used for intervals where the error is large, hence intervals that need refinement. The idea behind this operation is that the solutions $\{s_k^{\ell+1}\}_{k=1, \dots, N-1}$ between s_i^ℓ and s_{i+1}^ℓ are inserted and that the point s_{i+1}^ℓ is shifted such that $s_{i+1}^{\ell+1} = s_N^{\ell+1}$ and such that all points further than s_{i+1}^ℓ are updated to \tilde{s}_j^ℓ by the a shift using the distance between the last computed solution and the reference solution, i.e. $d(\Delta \mathbf{w}_N^{\ell+1})$, $\Delta \mathbf{w}_N^{\ell+1} = \mathbf{w}_{i+1}^\ell - \mathbf{w}_N^{\ell+1}$:

$$s_{k+1}^{\ell+1} = s_k^{\ell+1} + d(\Delta \mathbf{w}_k^{\ell+1}), \quad k = 0, \dots, N-1, \quad s_0^{\ell+1} = s_i^\ell, \quad s_{i+1}^{\ell+1} = s_N^{\ell+1}, \quad (15)$$

$$\xi_{k+1}^{\ell+1} = \xi_k^{\ell+1} + (\xi_{i+1}^\ell - \xi_i^\ell) \frac{s_{k+1}^{\ell+1} - s_k^{\ell+1}}{s_{i+1}^\ell - s_i^\ell}, \quad k = 0, \dots, N-1, \quad (16)$$

$$\tilde{s}_j^\ell = s_j^\ell + d(\mathbf{w}_N^{\ell+1}, \mathbf{w}_{i+1}^\ell), \quad j = i+1, \dots, I. \quad (17)$$

As can be noticed in equation (16), the re-scaling of ξ is done using the parametric length of the original interval at level ℓ , $(\xi_{i+1}^\ell - \xi_i^\ell)$ and the curve coordinate s_{i+1} relative to the beging point of the interval s_i with respect to the (updated) total curve length of the interval $s_{i+1} - s_i$, which is similar to the well-known *chord-length parameterization* in splines [22].

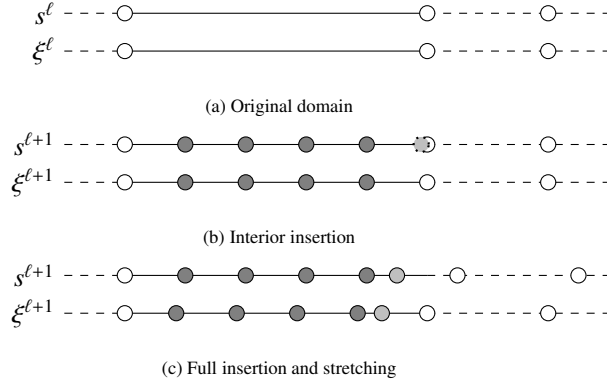


Figure 4: Domain parameterizations on the curve-length domain s and the parameter domain ξ with levels ℓ and $\ell + 1$. Figure 4a illustrates the original domain, figure 4b illustrates insertion of interior points in case of a sufficiently close approximation of the end-point of the domain and figure 4c illustrates the full insertion of all sub-domain solutions combined with the stretching of the curve length domain.

4. Implementation

In this section, data structures and algorithms for the implementation of the APALM are presented. In section 4.1 a data structure is provided for the implementation of the APALM. Thereafter, section 4.2 provides algorithms for the implementation of the APALM and section 4.3 elaborates on the extension of these methods to multiple branches, hence enabling arc-length exploration.

4.1. Data structure

Since the APALM is based on a sub-interval approach where the start- and end-point of each sub-interval are known, a data structure referencing the sub-intervals is essential. Since the curve-length coordinate is subject to change after reparameterization of the curve and since the curve parameter is fixed, the logical choice is to connect the data to parametric coordinates. That is, a series of discrete maps is constructed such that solutions, levels and curve-length coordinates can be obtained via a parametric point ξ_k^ℓ .

Figure 5 shows the data structure behind the APALM. Firstly the data structure contains the map $\mathcal{S}(\xi) : [0, 1] \rightarrow [0, S]$ which is the map that maps the parametric coordinate to the curve-length domain. Secondly, the maps $\mathcal{U}(\xi) : [0, 1] \rightarrow \mathbb{R}^{n+1}$ and $\mathcal{U}'(\xi) : [0, 1] \rightarrow \mathbb{R}^{n+1}$ map the solution and the previous solution from the parametric domain to the solution and previous solution domain, respectively. The mapper $\mathcal{U}'(\xi) : [0, 1] \rightarrow \mathbb{R}^{n+1}$ is constructed in order to construct the predictor of the ALM. Lastly, the map $\mathcal{L}(\xi) : [0, 1] \rightarrow \mathbb{N}$ is a map that can be used to obtain the level of a parametric point; which is optional but can be useful to limit the method to a certain depth.

4.2. Algorithms

Given the underlying data structure of the APALM, see section 4.1, algorithms are defined for its implementation. Firstly, it is assumed that the APALM is based on an ALM with possibly a black-box implementation, striving for

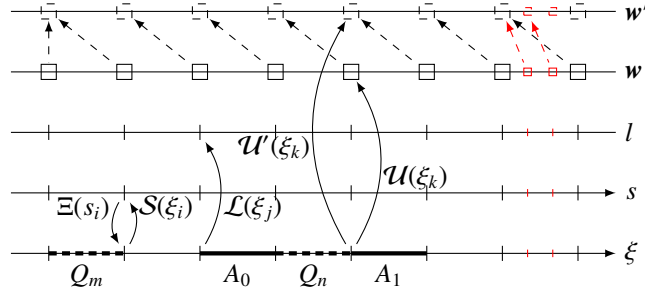


Figure 5: The data structure behind the APALM. The axes represent data sets, which are monotonically increasing when the axis has an arrow. Solid arrows represent mappers from an axis to another axis and dashed arrows represent data references. The mappers $\Xi(s_i)$ and $S(\xi_i)$ map between the curve parameterization and the curve length axes. The former takes a curve length s_i and returns the curve parameter ξ_i and the latter maps the inverse. The mappers $\mathcal{U}(\xi_k)$ and $\mathcal{U}'(\xi_k)$ return the solution w_j and the previous solution $(w')_j$, respectively, given a parametric coordinate ξ_j and the mapper $\mathcal{L}(\xi_j)$ returns the level on which the coordinate ξ_j was computed. The guess is a data reference to the previous solution. The thick solid intervals represent running jobs assigned with an ID and the thick dashed intervals represent queued intervals. Each interval is represented by a start-point and an end-point tuple (ξ_i, ξ_{i+1}) . The red lines, squares and arrows represent the `submit` operation when solutions are added to the data structure.

non-intrusiveness of the method. The required routines of the underlying ALM are:

- $w_{i+1}^\ell \leftarrow \text{step}(w_i^\ell, \Delta w_i^\ell \Delta L)$: Performs a step with length ΔL starting at point w_i^ℓ and returns the new solution w_{i+1}^ℓ . Given the current solution and the previous solution, a predictor for the initial iteration that employs $\Delta w_i^\ell = w_i^\ell - w_{i-1}^\ell$ could be available, as well as one for a cold start, i.e. $\Delta w_i^\ell = \mathbf{0}$.
- $\Delta s \leftarrow \text{distance}(w_i^\ell, w_j^\ell)$: gets the distance between two points w_i^ℓ and w_j^ℓ , using equation (2) with $\Delta w_i^\ell = w_i^\ell - w_j^\ell$.

In the following, a serial implementation of the APALM is presented, after which the parallel implementation will follow.

Serial implementation

The global workflow for a serial APALM, i.e. the AALM (adaptive arc-length method) is illustrated in algorithm 1. As seen in this algorithm, the initialization is performed using a `serialSolve` routine, which defines the initial solution sequence $\{w_i^0\}_{i=0}^I$ with I steps on level $\ell = 0$. In addition, this routines also provides a sequence of curve-length coordinates, $\{s_i^0\}_{i=0}^I$. Based on these sequences, the mappers from figure 5 and a queue Q is initialized in the `initializeMap` routine. Given the queue Q , the `solveQueue` routine provides a sequence of solutions $\{w_i\}$ and of curve parameters $\{s_i\}$ spanning multiple levels, hence the superscript ℓ is ommitted.

Algorithm 1 Global AALM routine (AALM). The AALM first consists of a serial solve of the whole curve length domain, followed by an evaluation of subintervals.

Input: $\Delta L, I$

- 1: $\{w_i^0\}_{i=0}^I, \{s_i^0\}_{i=0}^I \leftarrow \text{serialSolve}(\Delta L, I)$
- 2: $Q \leftarrow \text{initializeMap}(\{w_i^0\}_{i=0}^I, \{s_i^0\}_{i=0}^I)$
- 3: $\{w_i\}, \{s_i\} \leftarrow \text{solveQueue}(Q)$

Output: $\{w_i\}, \{s_i\}, \{\xi_i\}$

Using basic ALM routines, algorithm 2 defines an algorithm to obtain in serial a coarse approximation to initialize the AALM. Optionally, a stability computation can be performed after the arc-length step, which could lead to a specialized solve towards a bifurcation point. This allows for automatic exploration of bifurcation diagrams [8, 9] and is discussed more in detail in section 4.3.

Algorithm 2 Serial solve (`serialSolve`). This routine provides the initial step for the APALM/AALM, i.e. the solution data $\{\mathbf{w}_i^\ell\}_{i=0,\dots,I}$ and the corresponding curve-length parameters $\{s_i^\ell\}_{i=0,\dots,I}$ on level $\ell = 0$

Input: $\Delta L, I$

- 1: Initialize $\mathbf{w}_0^\ell, s_0^\ell = 0$
- 2: $\mathbf{w}_1^\ell \leftarrow \text{step}(\mathbf{w}_0^\ell, \mathbf{0}, \Delta L)$ ▷ Compute first solution
- 3: $s_1 \leftarrow \Delta L$
- 4: **for** $k = 1, \dots, I$ **do**
- 5: $\Delta \mathbf{w}_k^\ell = \mathbf{w}_k^\ell - \mathbf{w}_{k-1}^\ell$ ▷ Compute previous step
- 6: $\mathbf{w}_k^\ell \leftarrow \text{step}(\mathbf{w}_{k-1}^\ell, \Delta \mathbf{w}_k^\ell, \Delta L)$ ▷ Compute new solution
- 7: $s_k^\ell = s_{k-1}^\ell + \text{distance}(\mathbf{w}_k^\ell, \mathbf{w}_{k-1}^\ell)$ ▷ Compute curve coordinate
- 8: **end for**

Output: $\{\mathbf{w}_i^\ell\}_{i=0}^I, \{s_i^\ell\}_{i=0}^I$

As soon as a set of solution data and curve parameters, $\{\mathbf{w}_i^\ell\}_{i=0,\dots,I}$ and $\{s_i^\ell\}_{i=0,\dots,I}$, respectively, are known, the initialization of the parallel computations can take place. In this initialization, the maps from figure 5 are constructed and a queue Q of jobs is created, c.f. algorithm 3.

Algorithm 3 Parallel initialization (`initializeMap`). Within this algorithm, the maps $\mathcal{U}, \mathcal{U}', \mathcal{S}$ and Ξ are constructed from a series of solutions and corresponding curve length coordinates, $\{\mathbf{w}_i^\ell\}_{i=0}^I$ and $\{s_i^\ell\}_{i=0}^I$ respectively, both on level $\ell = 0$. Furthermore, the queue Q is initialized by adding all subintervals to the queue.

Input: $\{\mathbf{w}_i^\ell\}_{i=0}^I, \{s_i^\ell\}_{i=0}^I$

- 1: Add \mathbf{w}_0^ℓ to \mathcal{U} , s_0^ℓ to \mathcal{S} and ξ_0^ℓ to Ξ ▷ Add the start of the level 0 solutions to the map \mathcal{U}
- 2: **for** $k = 1, \dots, I$ **do**
- 3: Add \mathbf{w}_k^ℓ to \mathcal{U} and \mathbf{w}_{k-1}^ℓ to \mathcal{U}' .
- 4: Add s_k^ℓ to \mathcal{S} and ξ_k^0 to Ξ .
- 5: Add $Q_{k-1} = [\xi_{k-1}^\ell, \xi_k^\ell]$ to Q . ▷ Construct elements of the queue Q
- 6: **end for**

Output: $Q = \{Q_k = [\xi_k^\ell, \xi_{k+1}^\ell]\}_{k=0,\dots,I}$

After initialization, the computation of the sub-intervals can take place. This requires the routine `solveQueue` as defined in algorithm 4 for fully serial computations.

Algorithm 4 The routine that solves the queue (`solveQueue`). Given a queue Q , this algorithm takes an entry from the queue, using `pop` and solves the defined interval using `solveInterval`. The new solution is added to the solution maps and if required new jobs are added to the queue Q using `submit`. The final solutions are collected from the maps using the `collectSolutions` routine.

Input: Q

```

1: while  $Q \neq \emptyset$  do
2:    $Q, ID, \Delta L, \mathbf{w}_i^\ell, \mathbf{w}_{i-1}^\ell, \mathbf{w}_{i+1}^\ell \leftarrow \text{pop}(Q)$ 
3:    $\{d_k^{\ell+1}\}_{k=0, \dots, N-1}, \{\mathbf{w}_k^{\ell+1}\}_{k=0, \dots, N}, \overline{\Delta L}, \delta L \leftarrow \text{solveInterval}(N, \Delta L_0, \mathbf{w}_i^\ell, \mathbf{w}_{i-1}^\ell, \mathbf{w}_{i+1}^\ell)$ 
4:    $Q \leftarrow \text{submit}(ID, \{d_k^{\ell+1}\}_{k=0, \dots, N-1}, \{\mathbf{w}_k^{\ell+1}\}_{k=0, \dots, N}, \overline{\Delta L}, \delta L, Q)$    ▶ Submit the job; adds new jobs to  $Q$  if needed
5: end while
6:  $\{\mathbf{w}_i\}, \{s_i\} \leftarrow \text{collectSolutions}$ 

```

Output: $\{\mathbf{w}_i\}, \{s_i\}$

The computation of the sub-interval takes place in the `solveInterval` routine of algorithm 5 and can be used both in a serial and a parallel implementation. Given a number of sub-intervals N , the original distance between the end-points of the interval ΔL_0 and the start point, previous solution and reference solutions \mathbf{w}_i^ℓ , \mathbf{w}_{i-1}^ℓ and \mathbf{w}_{i+1}^ℓ , respectively, this routine computes a series of solutions of the sub-interval $\{\mathbf{w}_k^{\ell+1}\}_{k=0, \dots, N}$, their distances $\{d_k^{\ell+1}\}_{k=0, \dots, N-1}$ and the distances $\overline{\Delta L}$ and δL for error computation. Note that the distance $\Delta L'$ can be computed by taking the sum of the distances.

Algorithm 5 The routine that solves an interval (`solveInterval`). This routine takes a number of subintervals N , the desired step length for the total interval, the start point \mathbf{w}_i^ℓ , the previous point \mathbf{w}_{i-1}^ℓ and the next point \mathbf{w}_{i+1}^ℓ . It returns the solutions on the subinterval and the distances between them, respectively $\{d_j^{\ell+1}\}_{j=0, \dots, N-1}$ and $\{\mathbf{w}_j^{\ell+1}\}_{j=0, \dots, N}$, as well as the distances $\overline{\Delta L}$ and δL . When the step does not converge, it is assumed that step size modification takes place and that the data points are adjusted accordingly.

Input: $N, \Delta L_0, \mathbf{w}_i^\ell, \mathbf{w}_{i-1}^\ell, \mathbf{w}_{i+1}^\ell$

```

1: Initialize output vectors  $\{d_k^{\ell+1}\}_{k=0, \dots, N-1}, \{\mathbf{w}_k^{\ell+1}\}_{k=0, \dots, N}$ 
2:  $\Delta L = \Delta L_0 / N$    ▶ Defines the size of the sub-intervals
3:  $\Delta \mathbf{w}^\ell = \mathbf{w}_i^\ell - \mathbf{w}_{i-1}^\ell$    ▶ Determine previous arc-length step.
4: for  $k = 0, \dots, N - 1$  do
5:    $\mathbf{w}_{k+1} \leftarrow \text{step}(\mathbf{w}_k, \Delta \mathbf{w}, \Delta L)$    ▶ Perform the ALM iteration
6:    $\Delta \mathbf{w}_k^{\ell+1} = \mathbf{w}_{k+1}^{\ell+1} - \mathbf{w}_k^{\ell+1}$    ▶ Update the solution step
7:    $d_k \leftarrow \text{distance}(\mathbf{w}_{k+1}^{\ell+1}, \mathbf{w}_k^{\ell+1})$    ▶ Gets the distance
8: end for
9:  $\delta L \leftarrow \text{distance}(\mathbf{w}_{i+1}^\ell, \mathbf{w}_N^{\ell+1})$ 
10:  $\overline{\Delta L} \leftarrow \text{distance}(\mathbf{w}_N, \mathbf{w}_0)$ 

```

Output: $\{d_j^{\ell+1}\}_{j=0, \dots, N-1}, \{\mathbf{w}_j^{\ell+1}\}_{j=0, \dots, N}, \overline{\Delta L}, \delta L$

The `solveQueue` routine includes the `pop`, `submit` and `collectSolutions` routines. These routines mainly involve read and write operations for the mappers defined in figure 5, hence only a brief description is provided:

- $Q, ID, \Delta L, \mathbf{w}_i^\ell, \mathbf{w}_{i-1}^\ell, \mathbf{w}_{i+1}^\ell \leftarrow \text{pop}(Q)$: Takes the first available interval from the queue Q and returns a job ID, an interval length ΔL , the start solution \mathbf{w}_i^ℓ , the previous solution \mathbf{w}_{i-1}^ℓ and the next available solution \mathbf{w}_{i+1}^ℓ . It also updates the queue Q internally by removing the current entry.
- $Q \leftarrow \text{submit}(ID, \{d_k^{\ell+1}\}_{k=0, \dots, N-1}, \{\mathbf{w}_k^{\ell+1}\}_{k=0, \dots, N}, \overline{\Delta L}, \delta L, Q)$: Takes a job ID, the series of solutions $\{\mathbf{w}_k^{\ell+1}\}_{k=0, \dots, N}$ and their distances $\{d_k^{\ell+1}\}_{k=0, \dots, N-1}$ and the distances $\overline{\Delta L}$ and δL . Using equations (6) to (8), the errors are computed and solution intervals are added to the queue Q if needed.
- $\{\mathbf{w}_i\}, \{s_i\} \leftarrow \text{collectSolutions}$: Based on the underlying mappers, the solutions of all levels are collected into $\{\mathbf{w}_i\}$ and $\{s_i\}$.

Parallel implementation

For the implementation of the APALM, the `solveQueue` routine is re-defined and communications between workers and the manager are defined. Firstly, the global solution algorithm for the APALM is defined in algorithm 6. As for the AALM (see algorithm 1), the initialization is performed in serial by the `serialSolve` routine and the maps are initialized, both by the manager process. As soon as the queue Q is established, the queue can be processed in parallel.

Algorithm 6 Global APALM routine (APALM). The APALM first consists of a serial solve of the whole curve length domain, followed by a parallel evaluation of subintervals. This algorithm is specified for a simple manager-worker parallelization, more advanced parallelization schemes, e.g. with multiple managers, are easily achieved.

Input: $\Delta L, I$

```

1: if manager then
2:    $\{\mathbf{w}_i^\ell\}_{i=0}^I, \{s_i^\ell\}_{i=0}^I \leftarrow \text{serialSolve}(\Delta L, I)$ 
3:    $Q \leftarrow \text{initializeMap}(\{\mathbf{w}_i^\ell\}_{i=0}^I, \{s_i^\ell\}_{i=0}^I)$ 
4: else
5:   Wait
6: end if
7: if manager then
8:    $\{\mathbf{w}_i^\ell\}, \{s_i^\ell\} \leftarrow \text{solveQueue}(Q)$ 
9: else
10:  workerSolve()
11: end if

```

Output: $\{\mathbf{w}_i\}, \{s_i\}, \{\xi_i\}$

As seen in algorithm 6, the manager process uses the `solveQueue*` routine to manage the queue Q . This routine is presented in algorithm 7.

Algorithm 7 The `solveQueue*` routine, accompanied by the `workerSolve` routine from algorithm 8 and communication functions defined in table 1. This routine takes the queue Q and assigns jobs from the queue to the available workers. Then, while the queue Q is non-empty, data is communicated and to and from the workers and solutions are submitted. Note that the `pop` and `submit` routines are equivalent to the ones in algorithm 4.

Input: Q

```

1: Initialize a pool of worker processes  $W = \{W_j, j = 1, \dots, N_{\text{workers}}\}$ 
2: while  $Q \neq \emptyset$  and  $W \neq \emptyset$  do
3:    $Q, \text{ID}, \Delta L, \mathbf{w}_i^\ell, \mathbf{w}_{i-1}^\ell, \mathbf{w}_{i+1}^\ell \leftarrow \text{pop}(Q)$  ▷ See line 2 of algorithm 4
4:   sendStopManager2Worker(false)
5:   sendJobManager2Worker(ID,  $\Delta L_0, \mathbf{w}_i^\ell, \mathbf{w}_{i-1}^\ell, \mathbf{w}_{i+1}^\ell, W_j$ )
6:   Remove  $Q_i$  from  $Q$  and  $W_j$  from  $W$ 
7: end while
8: Send jobs to workers when they are available
9: while  $|W| \neq N_{\text{workers}}$  do
10:   $W_j, \text{ID}, \{d_j^{\ell+1}\}_{j=0, \dots, N-1}, \{\mathbf{w}_j^{\ell+1}\}_{j=0, \dots, N}, \overline{\Delta L}, \delta L \leftarrow \text{receiveDataWorker2Manager}$ 
11:   $Q \leftarrow \text{submit}(\text{ID}, \{d_j^{\ell+1}\}_{j=0, \dots, N-1}, \{\mathbf{w}_j^{\ell+1}\}_{j=0, \dots, N}, \overline{\Delta L}, \delta L, Q)$  ▷ See line 4 of algorithm 4
12:  Add  $W_j$  to  $W$ 
13:  while  $Q \neq \emptyset$  and  $W \neq \emptyset$  do
14:     $Q, \text{ID}, \Delta L, \mathbf{w}_i^\ell, \mathbf{w}_{i-1}^\ell, \mathbf{w}_{i+1}^\ell \leftarrow \text{pop}(Q)$ 
15:    sendStopManager2Worker(false)
16:    sendJobManager2Worker(ID,  $\Delta L_0, \mathbf{w}_i^\ell, \mathbf{w}_{i-1}^\ell, \mathbf{w}_{i+1}^\ell, W_j$ )
17:    Remove  $Q_i$  from  $Q$  and  $W_j$  from  $W$ 
18:  end while
19: end while
20: sendStopManager2All(true)

```

Output: $\{\mathbf{w}_i\}, \{s_i\}$

The worker processes will perform the `workerSolve` from algorithm 8. This algorithm is very similar to the serial `solveQueue`, but the differences include communications of data as well as a stop signal. The latter is broadcasted to all workers as soon as the queue Q is empty.

Algorithm 8 Solve routine for a worker (`workerSolve`). This routine is very similar to algorithm 4, except the addition of communications to the manager process, which are defined in table 1

Input:

```

1: Initialize stop = false
2: while true do
3:   stop ← receiveStopManager2Worker
4:   if stop then
5:     Break loop
6:   end if
7:   (ID, ΔL0, wi, wi-1, wref) ← receiveJobManager2Worker
8:   {dkℓ+1}k=0,...,N-1, {wkℓ+1}k=0,...,N, ΔL̄, δL ← solveInterval(N, ΔL0, wiℓ, wi-1ℓ, wi+1ℓ)
9:   sendDataWorker2Manager(ID, {dj}j=0,...,N-1, {wj}j=0,...,N, ΔL̄)
10: end while

```

Output:

As can be seen in algorithm 7 and algorithm 8, the `solveQueue*` and `workerSolve` routines rely on process communication. In particular, these communication routines are defined in table 1.

Table 1: Required communications between manager and worker processes for the APALM.

Send/Receive	Data	Description
sendJobManager2Worker receiveJobManager2Worker	ID, ΔL ₀ , w _i ^ℓ , w _{i-1} ^ℓ , w _{i+1} ^ℓ	Communicates information to perform the computation of an interval between the manager and the worker processes.
sendDataWorker2Manager receiveDataWorker2Manager	W _j , ID, {d _j ^{ℓ+1} } _{j=0,...,N-1} , {w _j ^{ℓ+1} } _{j=0,...,N} , ΔL̄, δL	Communicates the data resulting from a sub-interval computation between the manager and the worker processes. The receive communication also provides the worker from which the data is received.
sendStopManager2All receiveStopManager2Worker	Boolean	Communicates a stop signal between the manager and the worker processes.

4.3. Arc-length exploration

To enable multi-branch parallelization of APALM, small modifications are required to the data structure and the algorithms presented in sections 4.1 and 4.2. The easiest multi-branch parallelization is achieved by identifying branch-switches only in the serial solve such that the initialization of the APALM can be done across different branches. In this case, the serial solve is performed on the main branch and any bifurcation point is stored such that a restart can be

performed from this point, see [9] for details. As soon as such a bifurcation point is identified, a branch switch can be performed and a new serial solve can be started from that point. As a result, a series of solutions $\{\mathbf{w}_i\}_{i=0}^l$ is computed for each branch. Similar to the single-branch case, a data structure and a queue can be initialized using algorithm 3 per branch. Depending on the parallel configuration, the queues Q^b , $b = 0, \dots, n_{\text{branches}}$ of all branches can be treated separately by multiple manager processes, or they can be combined into one large queue Q and be handled by one single manager process. In the latter case, each job will contain also a branch identifier to refer to the corresponding data structure.

The advantages of the above approach combining multi-branch and within-branch parallelization using the APALM is that the extension from a single-branch APALM to a multi-branch APALM is straightforward. The disadvantage, however, is that the identification of bifurcations is only taken into account in the serial solve step, hence any bifurcations that are identified in the parallel solve will not be taken into account. A remedy would be to rebuild the map and the data structure on the manager process as soon as a worker process finds a bifurcation point; this requires all active workers to terminate.

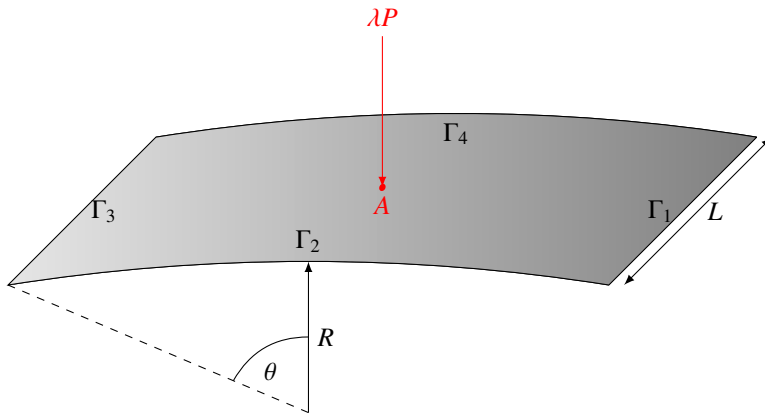
5. Numerical Experiments

In this section, the APALM scheme is demonstrated on a series of benchmark problems. The first two benchmark problems are structural analysis problems with limit-point instabilities and complex collapsing mechanisms involving strongly curved solution paths. The third benchmark is a buckling problem, containing a bifurcation with multiple branches to illustrate the concept of the APALM in a multi-branch setting. All benchmark problems are computed using isogeometric Kirchhoff-Love shell elements based on the works [23–25]. Furthermore, a scaling test with respect to the number of workers is performed for all benchmark problems. Here, the communications from table 1 are performed using the Message Passing Interface (MPI) and within the job serial computations are performed. The computations are performed on the Delft High Performance Computing Centre (DHPC) [26] with Intel XEON E5-6248R 24C 3.0GHz nodes with 96GB memory per CPU. The code is made available within the Geometry + Simulation modules [27] library and instructions for reproduction of the results of this paper can be found on ([URL will be made available upon publication](#)).

5.1. Collapse of a shallow roof

The first benchmark problem involves a shallow roof subject to a point-load in the mid-point. The roof is discretized with 4×4 NURBS elements of degree 3. The roof is composed of a lay-up of composites with material properties as presented in figure 6, inspired by [28]. It is modelled using isogeometric Kirchhoff-Love shell elements [23] supporting composite laminates [29]. A Crisfield ALM is used with initial arc-length of 30 and a scaling parameter $\Psi = 1$. The tolerance of the APALM is set to $\varepsilon_l = \varepsilon_u = 10^{-2}$. More geometric, material and load parameters can be found in figure 6. Reference solutions are obtained using a serial arc-length method with a sufficiently fine increment size.

Figure 7 provides the results of the APALM applied to the collapse of the shallow roof. As can be seen from this



Boundary conditions		
Γ_1, Γ_3	$u_x = u_y = u_z = 0$	
Γ_2, Γ_4	Free	
Geometric parameters		
L	508	[mm]
R	2540	[mm]
t	6.35	[mm]
θ	10	[rad]
Material parameters (Saint-Venant Kirchhoff laminate)		
E_{11}	3300	[N/mm ²]
E_{22}, E_{33}	1100	[N/mm ²]
G_{12}, E_{13}	660	[N/mm ²]
E_{23}	440	[N/mm ²]
$\nu_{12}, \nu_{13}, \nu_{23}$	0.25	[-]
Lay-up	[0/90/0]	[°]
Loads		
P	10	[N]
λ	variable	[-]

Figure 6: Geometry (left) and problem details (right) for the benchmark problem of the collapse of a composite shallow cylindrical roof. The reference deformations are obtained in the mid-point denoted by A and the load P is scaled by load factor λ and is applied in the same point. The displacements are fixed in all direction on both sides Γ_1 and Γ_3 and free on the other boundaries.

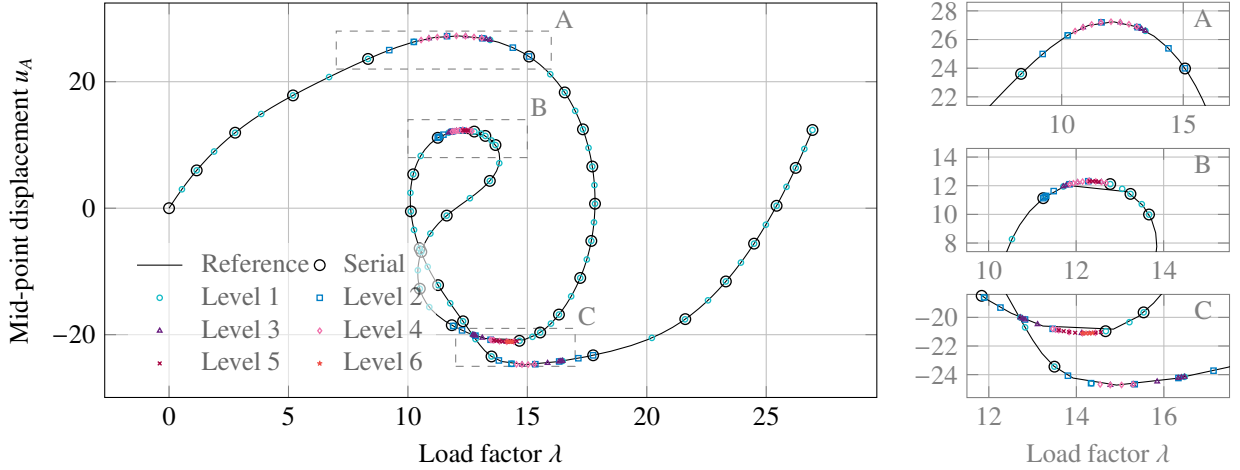
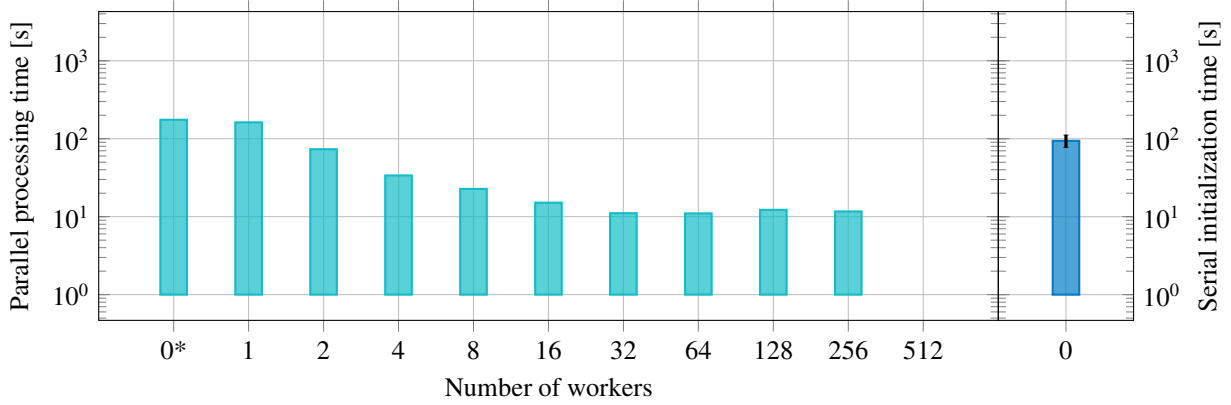


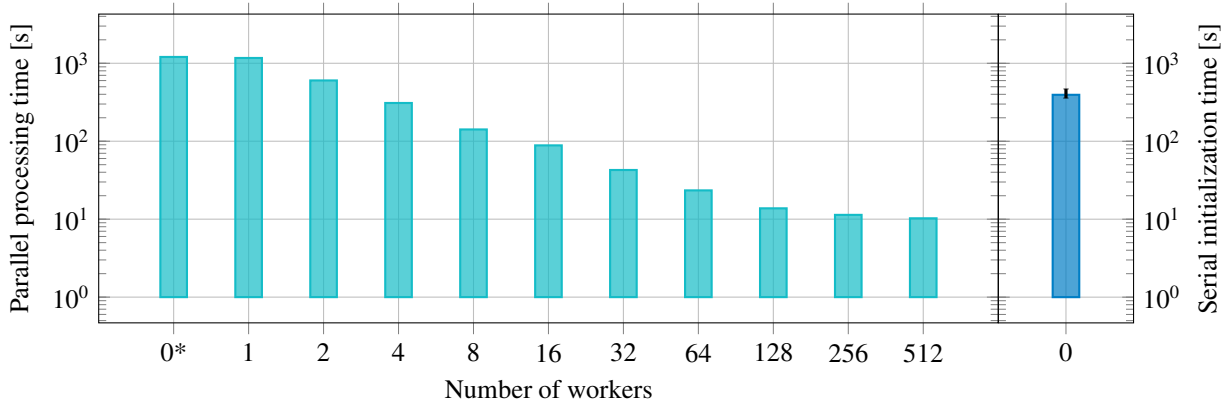
Figure 7: Results of the collapsing roof. The figure on the left indicates the full solution path and the figures on the right depict the insets indicated in the left figure. The reference and serial solutions are represented by respectively the solid line and the black markers. The solutions computed by the APALM are indicated per level. The simulation is performed with a tolerance of $\varepsilon_l = \varepsilon_u = 10^{-2}$ and a increment length of $\Delta L = 30$.

figure, the serial computation provides a coarse estimate of the reference curve. Especially on the first limit point (between $\lambda \times w_A \in [-15, -8] \times [20, 25]$) the data is sparse, similar to the collapse itself (see inset in figure 7). The results of the APALM show that a lot of refinements are needed to represent the collapsing behaviour correctly in the region of the inset in figure 7. These regions do not necessarily involve extremely curved paths in the axes of figure 7, but the solutions w are most likely curved in the higher-dimensional solution space.

In order to assess the parallelization of the APALM in this example, the test from figure 7 is performed with an increasing number of workers. That is, the serial initialization is performed on the manager process after which the parallel computations are performed on a given number of workers. In figure 8, the parallel computation time for a fixed number of workers is presented. In addition, the time for serial initialization is given as an average of multiple runs. From figure 8a, it can be seen that for the run with the same APALM parameters as in figure 7, the parallel evaluation scales expectedly until 32 workers. Doubling the number of workers further does not increase the parallel processing time. In addition, it can be seen that with 32 or more workers, the parallel evaluations are about 10% of the time of the serial initialization. The reason for the stagnation of the parallel processing time is related to the initial length of the queue of jobs, resulting from the serial initialization phase. In this case, 50 intervals have been initialized, meaning that the parallel computation phase is initiated with 50 workers maximum. Adding more workers than 50 hardly increases the scalability of the method. Indeed, looking at figure 8b, populating the initial queue with more than 600 intervals yields optimal scalability for up to at least 256 workers. Running the same simulation with 512 cores, however, does not greatly improve with respect to 256 workers. This can be explained by the fact that for this particular case, there are not many jobs resulting from the first jobs that are performed in parallel, meaning that most of the workers are idle after their first computed interval resulting from the serial initialization. Lastly, as can be seen from both graphs in figure 8, the difference between a fully serial (i.e. without communications) and a parallel processing with a single worker (i.e. serial



(a) The serial initialization phase consists of 51 data points, and the parallel corrections consist of 191 data points. The simulation is performed with a tolerance of $\varepsilon_l = \varepsilon_u = 10^{-2}$ and a increment length of $\Delta L = 30$, as in figure 10.



(b) The serial initialization phase consists of 601 data points, and the parallel corrections consist of 2001 data points. The simulation is performed with a tolerance of $\varepsilon_l = \varepsilon_u = 10^{-4}$ and a increment length of $\Delta L = 2.5$

Figure 8: Parallel processing times for the collapsing roof. The horizontal axis presents the number of workers, where the 0* indicates a process without MPI communications and the other numbers represent the number of MPI processes in addition to the main process. The vertical axis on the left presents the time for parallel processing after the serial initialization phase. The vertical axis on the right provides the average time required for serial initialization, where the error bar represents the variation of the serial initialization time for all performed runs.

but with communication) is negligible. This shows that the communication overhead is negligible as well. Nevertheless, the results from figure 8b show that given an available serial approximation, a parallel and adaptive correction can be performed in a fraction (2.5%) of the serial computation time.

5.2. Collapse of a truncated cone

The second benchmark example is based on [25] and involves the collapsing behaviour of a truncated cone with a hyperelastic Mooney-Rivlin material model. This benchmark is based on [30] but in the work of [25] the full collapsing behaviour was revealed using arc-length methods. The geometry, material and load specifications can be found in figure 9.

The truncated cone is modelled using a quarter geometry using symmetry conditions to represent the axisymmetry

as used in the original case of [30]. The geometry is modelled with 32 NURBS elements of degree 2 over the height. Furthermore, an initial arc-length of 0.5 is used and the scaling factor is $\Psi = 0$. The top boundary Γ_2 is free and on the bottom boundary Γ_4 all displacements are fixed. The other boundaries have symmetry boundary conditions. The governing material model is an incompressible Mooney-Rivlin material model with strain energy density function (with slight abuse of notation)

$$\Psi(\mathbf{C}) = \frac{c_1}{2} (I_1 - 3) + \frac{c_2}{2} (I_2 - 3), \quad (18)$$

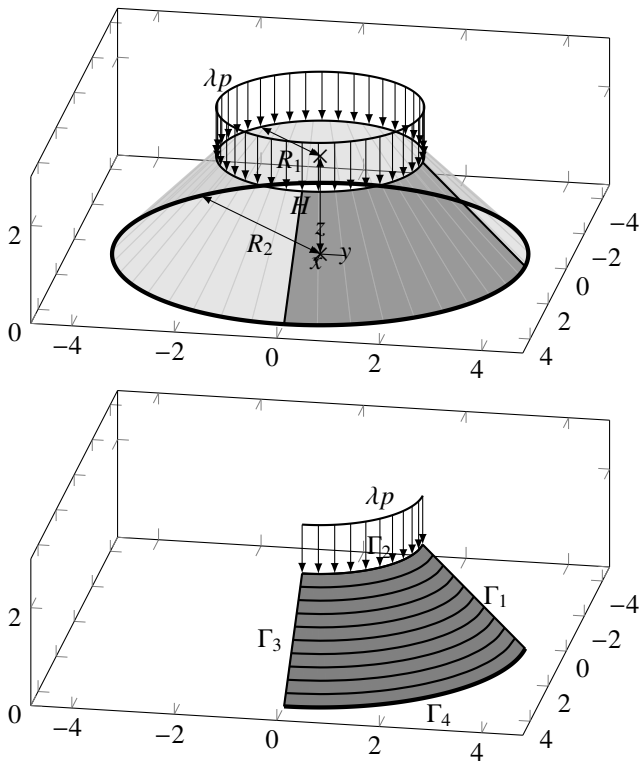
with I_1 and I_2 the first and second invariants of the deformation tensor $\mathbf{C} = \mathbf{F}^T \mathbf{F}$. More information on the problem set-up and the material models can be found in [25]. The reference results are obtained from a serial ALM computation with a sufficiently small increment size.

The results of the collapsing truncated cone problem are presented in figure 10. As seen in this picture, the serial initialization provides a coarse approximation of the path, but leaves out details, e.g., the rotated “S”-shaped curve in the inset in figure 10. From the results, it is clear that the APALM focusses its refinement on the curved parts of the path, and reveals the “S”-shaped curve among other features of the path.

Similar to the collapse of the roof, a scaling analysis of the parallel evaluations is performed. In figure 11 the processing times of the serial initialization and the parallel correction phase are presented for the collapsing truncated cone with different APALM parameters. Firstly figure 11a provides the parallel processing times for the parameters as used to obtain figure 10. As can be seen in this figure, the parallel scaling for 81 intervals stops when using 32 workers or more. This is explained by the fact that the solution curve of the present example consists of a small number of very fine regions, which are generally found through a series of newly added jobs in the queue. When the number of intervals in the serial initialization is increased to 640 intervals, it can be seen that the parallel processing step scales very well. In this case, the number of jobs in the initial queue is big enough to activate all workers after serial initialization. Also, it is found that the depth of the adaptive intervals is only 3 levels in contrast to 6 levels in case of figure 10. This means that the simulation has less dependencies in the queue, increasing the scalability of the parallel processing stage. However, it should be noted that in that case, the need for adaptivity is less.

5.3. Strip buckling

As a last example, a benchmark problem involving a bifurcation is presented. The problem consists of a flat strip that is clamped on one edge and free on all the other, with an in-plane compressive load applied on the free end opposite to the clamped edge, see figure 12 for the problem set-up and [31] for the reference results. The ALM that is used is a Crisfield method with $\Psi = 0$, with a pre-buckling arc-length of $5 \cdot 10^{-5}$, a post-buckling arc-length of 5 and a tolerance of the APALM of $\varepsilon_l = \varepsilon_u = 10^{-3}$. The serial ALM is equipped with an extension for the computation of singular points [5], see [32] for more details on this implementation. Using these methods, an initially flat strip is compressed until the bifurcation point has been computed. As soon as the strip becomes unstable, the bifurcation point is computed and a branch switch is performed, marking the transition between the pre-buckling and post-buckling branches.



Boundary conditions		
Γ_1	Symmetry	
Γ_2	Free	
Γ_3	Symmetry	
Γ_4	$u_x = u_y = u_z = 0$	
Geometric parameters		
H	1	[m]
R_1	1	[m]
R_2	2	[m]
t	0.1	[m]
Material parameters (Incompressible Mooney-Rivlin)		
$\mu = c_1 + c_2$	4.225	[N/mm ²]
c_1/c_2	7	[-]
Loads		
p	1	[N/m]
λ	variable	[N]

Figure 9: Geometry (left) and problem details (right) for the benchmark problem of the collapsing truncated cone. The cone is modelled by using a quarter of the geometry, using symmetry conditions. The displacements are fixed in all direction on the bottom boundary and the cone and the top boundary is subject to a line load.

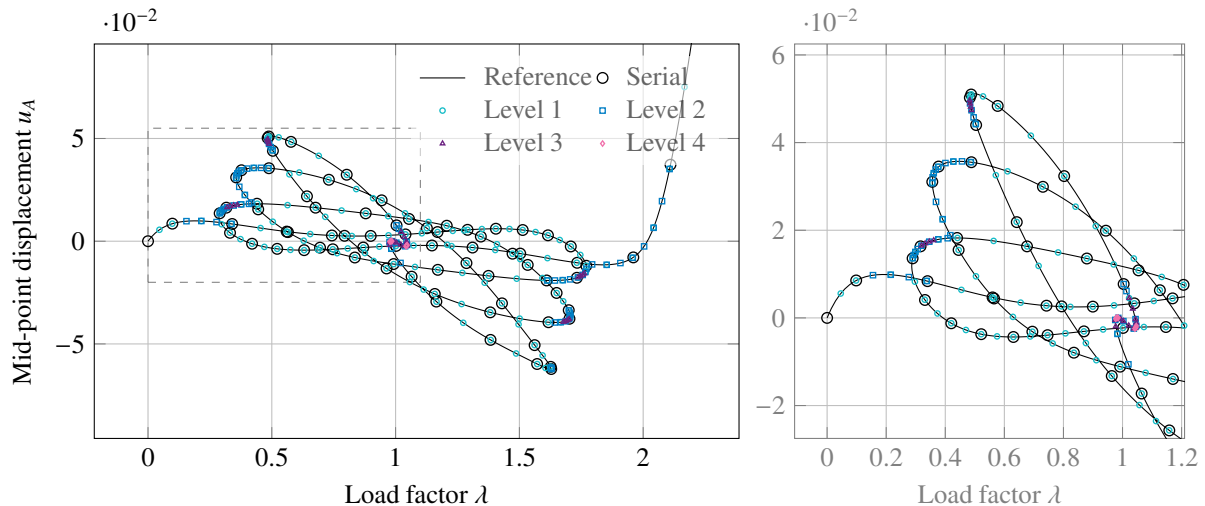


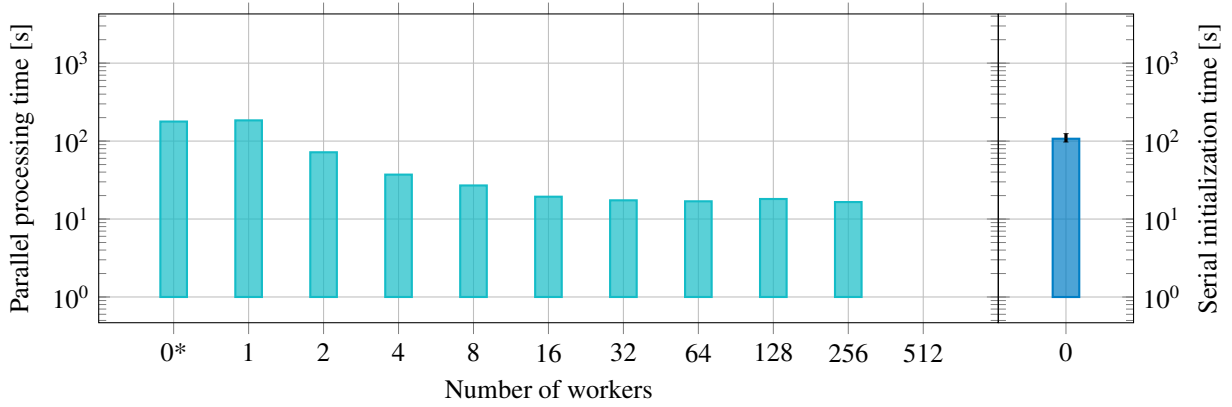
Figure 10: Results of the collapsing truncated cone. The figure on the left depicts the full solution path and the figure on the right depicts the inset indicated in the left figure. The reference and serial solutions are represented by respectively the solid line and the black markers. The solutions computed by the APALM are indicated per level. The simulation is performed with a tolerance $\varepsilon_l = \varepsilon_u = 10^{-2}$ and a increment length of $\Delta L = 0.5$.

The results for the buckled strip are presented in figure 13. In this figure, the non-dimensional horizontal and vertical displacements of the end-point are plotted with respect to the non-dimensional applied load. In the plots, the pre- and post-buckling branches are plotted separately for clarity, but the branches should obviously be connected at the bifurcation point. As can be seen from the results, a rather coarse serial approximation of the post-buckling branch gives a good starting point for a multi-level approximation of the curve, providing additional detail in the sharp corner in $W/L \in [0.7, 0.8]$. In addition, it can be seen that the pre-buckling branch requires no more levels than the first, as the behaviour there is just a linear axial compression, hence the solution path is straight.

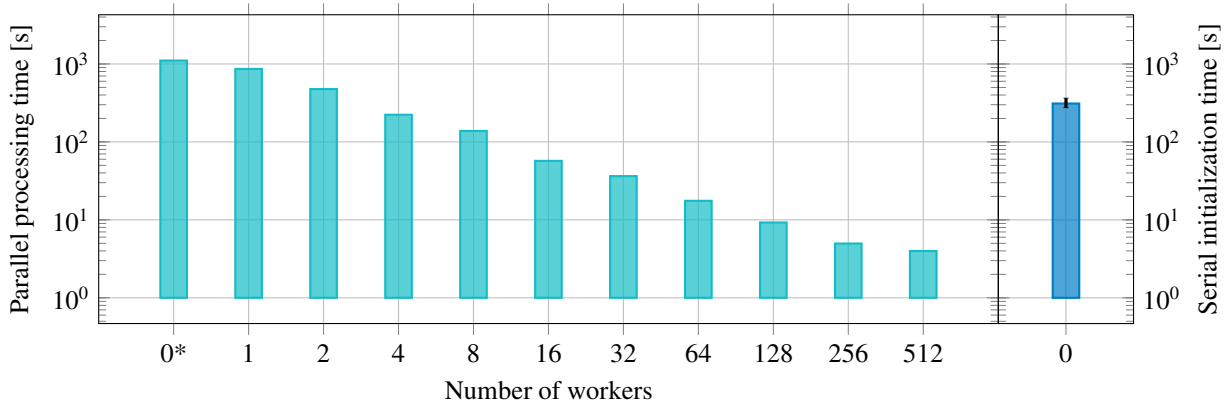
In figure 14, the parallel processing time and the serial initialization time is provided for the buckled strip. From these figures, similar conclusions as from the previous two examples can be drawn. That is, the parallel scalability improves when increasing the initial number of intervals. In this case, the parallel processing time scales very well until 16 workers, although the initialization only consists of 7 intervals. This is due to the fact that the difference in the number of intervals between the serial initialization and the parallel correction for the post-buckling is relatively large, meaning that the adaptivity algorithm provides a large number of jobs. Furthermore, it can be seen that the scalability of the parallel stage of the APALM is not affected by the bifurcation problem. This is due to the fact that the worker processes are not limited to a single branch, but they compute jobs on all branches.

6. Conclusions and outlook

In this paper, an Adaptive Parallel Arc-Length Method (APALM) is presented. Contrary to existing parallel implementations of the Arc-Length Method (ALM), the present method provides a within-branch parallelization, hence provides scalable parallelization independent of the physics of the problem, i.e. the number of branches. The method employs a multi-level approach, where parallelization is started after a serial initialization phase. Then, given the sub-

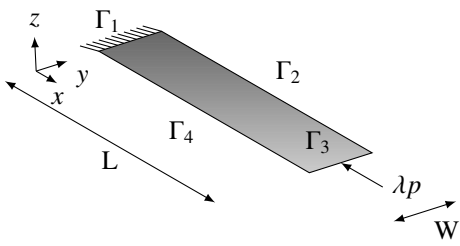


(a) The serial initialization phase consists of 82 data points, and the parallel corrections consist of 264 data points. The simulation is performed with a tolerance $\varepsilon_l = \varepsilon_u = 10^{-2}$ and a step length of $\Delta L = 0.5$, as in figure 10.



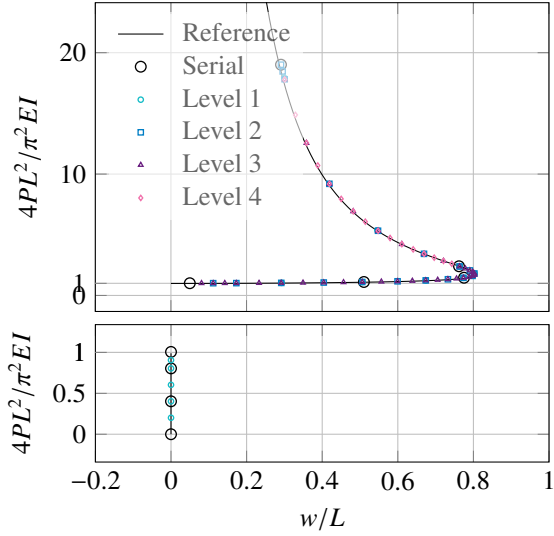
(b) The serial initialization phase consists of 641 data points, and the parallel corrections consist of 2001 data points. The simulation is performed with a tolerance $\varepsilon_l = \varepsilon_u = 10^{-4}$ and a step length of $\Delta L = 6.25 \cdot 10^{-2}$.

Figure 11: Parallel processing times for the collapsing truncated cone. The horizontal axis presents the number of workers, where the 0* indicates a process without MPI communications and the other numbers represent the number of MPI processes in addition to the main process. The vertical axis on the left presents the time for parallel processing after the serial initialization phase. The vertical axis on the right provides the average time required for serial initialization, where the error bar represents the variation of the serial initialization time for all performed runs.

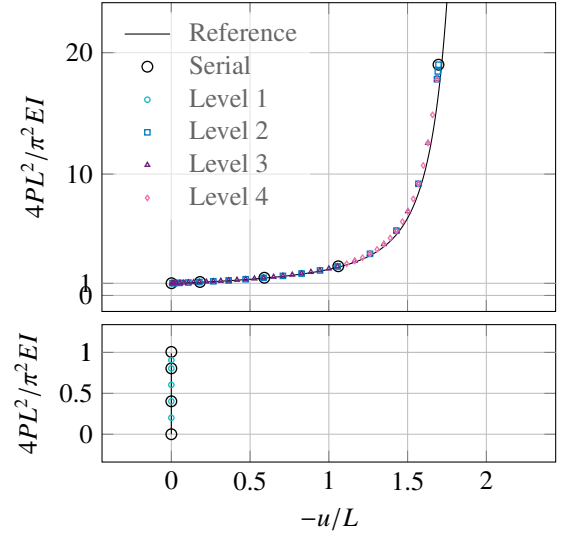


Boundary conditions		
Γ_1	$u_x = u_y = u_z = \theta_x = \theta_y = \theta_z = 0$	
Γ_2	$u_y = 0$	
Γ_3	u_x, u_y, u_z coupled	
Γ_4	$u_y = 0$	
Geometric parameters		
L	1	[m]
W	0.01	[m]
t	0.01	[m]
Material parameters (Saint-Venant Kirchhoff)		
E	$75 \cdot 10^6$	[N/mm ²]
ν	0	[-]
Loads		
p	0.1	[N]
λ	variable	[N]

Figure 12: Geometry (left) and problem details (right) for the buckling of a strip subject to a horizontal load. One end of the strip is fully fixed (displacements and rotations) and the other end is free but subject to an in-plane compressive load.



(a) Non-dimensional out-of-plane displacement of the beam with respect to the non-dimensional buckling load.

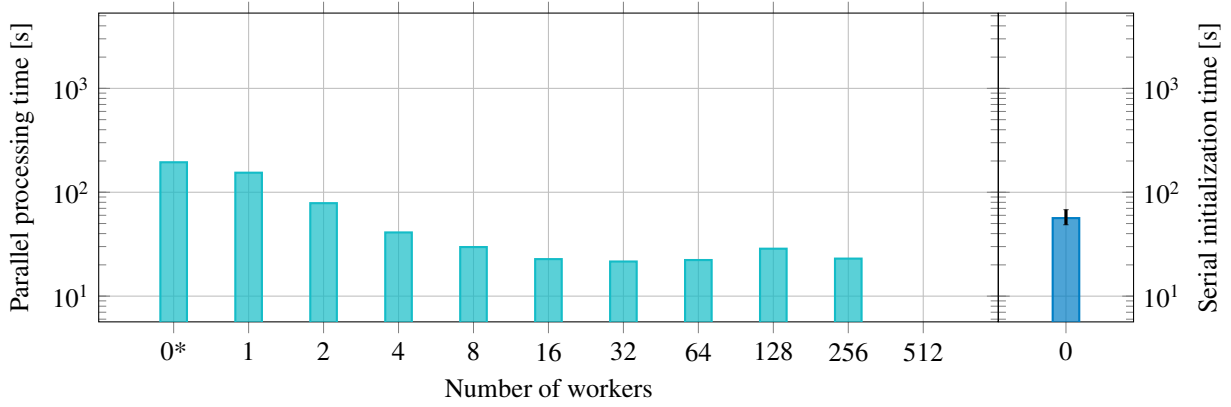


(b) Non-dimensional in-of-plane displacement (length direction) of the beam with respect to the non-dimensional buckling load.

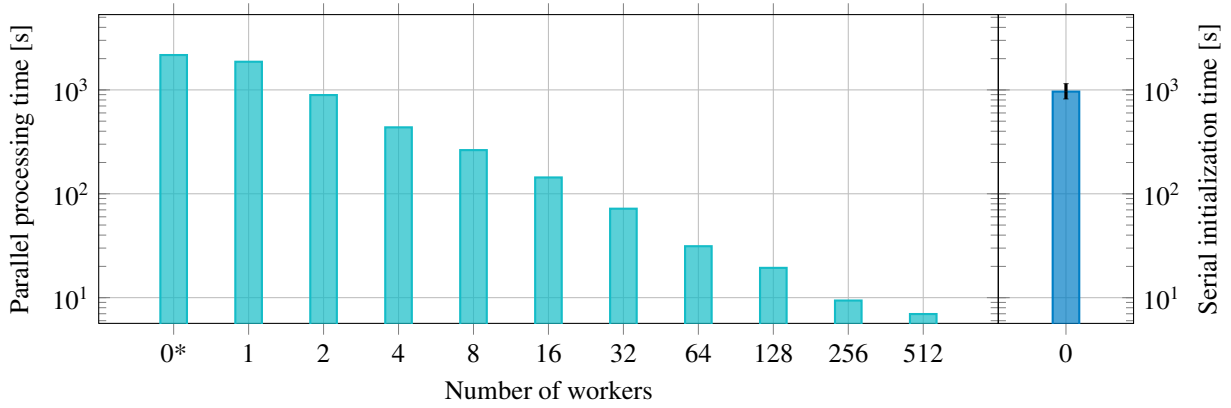
Figure 13: Results of the buckling of a clamped strip. The left figure provides the out-of-plane displacement of the free end with respect to the non-dimensional load $4PL^2/\pi^2EI$ and the right figure represents the horizontal displacement of the free end with respect to the same non-dimensional load. In both figures, buckling occurs when $4PL^2/\pi^2EI = 1$ and the axes are split on this point to make the pre- and post-buckling branches both visible. The simulation is performed with a tolerance $\varepsilon_l = \varepsilon_u = 10^{-3}$ and a step length of $\Delta L = 5 \cdot 10^{-5}$ (pre-buckling) and $\Delta L = 5$ (post-buckling).

intervals provided by the serial computation, computations with finer arc-lengths can be performed and evaluated using suitable error measures; marking intervals for further refinement when needed. Given a basic step function and distance computation, the present paper provides all algorithms necessary for implementing the APALM with a manager-worker parallelization.

The implementation of the APALM is evaluated using three benchmark problems. The first problem involves the collapse of a composite shallow cylindrical shell. The second problem involves the collapse of a truncated conical rubber shell and the third example involves a bifurcation problem of a strip subject to an in-plane load. In all examples, it can be observed that the APALM provides an accurate description of the reference solution, given a (sufficiently) coarse serial initialization of the curve. Through refinement, the APALM provides refinements (hence details in the solution) typically on sharp corners in the load-displacement diagrams. In addition, the bifurcation example also shows that the APALM is able to work within an exploration scheme for bifurcations. Lastly, all benchmark problems have been evaluated on their scalability within the parallel evaluation stage following the serial initialization. From these experiments, it can be concluded that the parallel processing time of the APALM decreases with the number of workers when the number of intervals from serial initialization is greater or equal to the number of workers, or in cases when there is strong adaptivity resulting from the APALM. Only the former provides a rule of thumb to select a number of workers since it is known *a priori*. Furthermore, it can be seen that the parallel processing time scales well for a low number of workers, meaning that the method is already beneficial on desktop scale. In general, the parallelization of the APALM can be improved by



(a) The serial initialization phase consists of 4 data points in the pre-buckling branch and 5 data points in the post-buckling branch. The parallel corrections consist of 6 data points in the pre-buckling branch and 88 data points in the post-buckling branch. The simulation is performed with a tolerance of $\varepsilon_l = \varepsilon_u = 10^{-3}$ and a step length of $\Delta L = 5 \cdot 10^{-5}$ (pre-buckling) and $\Delta L = 5$ (post-buckling), as in figure 13b.



(b) The serial initialization phase consists of 252 data points in the pre-buckling branch and 334 data points in the post-buckling branch. The parallel corrections consist of 502 data points in the pre-buckling branch and 1498 data points in the post-buckling branch. The simulation is performed with a tolerance of $\varepsilon_l = \varepsilon_u = 10^{-5}$ and a step length of $\Delta L = 5 \cdot 10^{-7}$ (pre-buckling) and $\Delta L = 5 \cdot 10^{-2}$ (post-buckling).

Figure 14: Parallel processing times for the strip buckling example. The horizontal axis presents the number of workers, where the 0* indicates a process without MPI communications and the other numbers represent the number of MPI processes in addition to the main process. The vertical axis on the left presents the time for parallel processing after the serial initialization phase. The vertical axis on the right provides the average time required for serial initialization, where the error bar represents the variation of the serial initialization time for all performed runs.

using dynamic load balancing within OpenMP.

As the APALM enables parallelization in the arc-length domain, future applications of this method include quasi-static computations for solid and fluid-dynamics among other problems, especially the ones with a large number of load steps. Therefore, future works with this method include automatic exploration of solution spaces, e.g., following the work of [8, 9], or applications with large numbers of degrees of freedom, for instance with phase-field models for fracture mechanics [33]. Other future work includes combining the APALM with a spatial refinement scheme, to enable space-quasi-time refinements. Lastly, MPI scalability and distribution of cores per worker are topics to investigate for different applications.

Acknowledgments

The authors are grateful for the financial support from Delft University of Technology.

References

- [1] K. Rupp, M. Horovitz, F. Labonte, O. Shacham, K. Olukotun, L. Hammond, C. Batten, Years of microprocessor trend data, Figure available on webpage [http://www.karlsruhp.net/wp-content/uploads/2015_6\(42\)40](http://www.karlsruhp.net/wp-content/uploads/2015_6(42)40).
- [2] M. J. Gander, 50 Years of Time Parallel Time Integration (2015) 69–113.
- [3] E. Riks, The Application of Newton’s Method to the Problem of Elastic Stability, *Journal of Applied Mechanics* 39 (1972) 1060.
- [4] M. M. Crisfield, A Fast Incremental/Iterative Solution Procedure That Handles “Snap-Through”, in: *Computational Methods in Nonlinear Structural and Solid Mechanics*, Pergamon, 1981, pp. 55–62.
- [5] P. Wriggers, W. Wagner, C. Miehe, A quadratically convergent procedure for the calculation of stability points in finite element analysis, *Computer Methods in Applied Mechanics and Engineering* 70 (1988) 329–347.
- [6] G. Pretti, W. M. Coombs, C. E. Augarde, A displacement-controlled arc-length solution scheme, *Computers & Structures* 258 (2022) 106674.
- [7] C. Kadapa, A simple extrapolated predictor for overcoming the starting and tracking issues in the arc-length method for nonlinear structural mechanics, *Engineering Structures* 234 (2021) 111755.
- [8] J. Thies, M. Wouters, R. S. Hennig, W. Vanroose, Towards Scalable Automatic Exploration of Bifurcation Diagrams for Large-Scale Applications, *Lecture Notes in Computational Science and Engineering* 139 (2021) 981–989.
- [9] M. Wouters, W. Vanroose, Automatic Exploration Techniques of Numerical Bifurcation Diagrams Illustrated by the Ginzburg–Landau Equation, https://doi.org/10.1137/19M1248467_18 (2019) 2047–2098.
- [10] J. L. Lions, Y. Maday, G. Turinici, Résolution d’EDP par un schéma en temps $\ddot{\imath}$ parallél $\ddot{\imath}\ddot{\imath}$, *Comptes Rendus de l’Académie des Sciences - Series I - Mathematics* 332 (2001) 661–668.
- [11] R. D. Falgout, S. Friedhoff, T. V. Kolev, S. P. MacLachlan, J. B. Schroder, Parallel time integration with multigrid, *SIAM Journal on Scientific Computing* 36 (2014) C635–C661.
- [12] E. C. Cyr, S. Günther, J. B. Schroder, Multilevel initialization for layer-parallel deep neural network training, *arXiv preprint arXiv:1912.08974* (2019).
- [13] A. Hessenthaler, R. D. Falgout, J. B. Schroder, A. de Vecchi, D. Nordsletten, O. Röhrle, Time-periodic steady-state solution of fluid-structure interaction and cardiac flow problems through multigrid-reduction-in-time, *arXiv preprint arXiv:2105.00305* (2021).
- [14] D. A. Aruliah, L. Van Veen, A. Dubitski, Algorithm 956: PAMPAC, a parallel adaptive method for pseudo-arclength continuation, *ACM Transactions on Mathematical Software* 42 (2016).
- [15] M. Ritto-Corrêa, D. Camotim, On the arc-length and other quadratic control methods: Established, less known and new implementation procedures, *Computers and Structures* 86 (2008) 1353–1368.
- [16] S. A. Ragon, Z. Gürdal, L. T. Watson, A comparison of three algorithms for tracing nonlinear equilibrium paths of structural systems, *International Journal of Solids and Structures* 39 (2002) 689–698.

- [17] K. Schweizerhof, P. Wriggers, Consistent linearization for path following methods in nonlinear fe analysis, *Computer Methods in Applied Mechanics and Engineering* 59 (1986) 261–279.
- [18] P. Bellini, A. Chulya, An improved automatic incremental algorithm for the efficient solution of nonlinear finite element equations, *Computers & Structures* 26 (1987) 99–110.
- [19] E. Carrera, A study on arc-length-type methods and their operation failures illustrated by a simple model, *Computers and Structures* 50 (1994) 217–229.
- [20] W. F. Lam, C. T. Morley, Arc-Length Method for Passing Limit Points in Structural Calculation, *Journal of Structural Engineering* 118 (1992) 169–185.
- [21] Z. Zhou, D. Murray, An incremental solution technique for unstable equilibrium paths of shell structures, *Computers and Structures* 55 (1995) 749–759.
- [22] L. Piegl, W. Tiller, *The NURBS Book*, Monographs in Visual Communications, Springer Berlin Heidelberg, Berlin, Heidelberg, 1995. doi:10.1007/978-3-642-97385-7.
- [23] J. Kiendl, K.-U. Bletzinger, J. Linhard, R. Wüchner, Isogeometric shell analysis with Kirchhoff–Love elements, *Computer Methods in Applied Mechanics and Engineering* 198 (2009) 3902–3914.
- [24] J. Kiendl, M.-C. Hsu, M. C. Wu, A. Reali, Isogeometric Kirchhoff–Love shell formulations for general hyperelastic materials, *Computer Methods in Applied Mechanics and Engineering* 291 (2015) 280–303.
- [25] H. Verhelst, M. Möller, J. Den Besten, A. Mantzaflaris, M. Kaminski, Stretch-Based Hyperelastic Material Formulations for Isogeometric Kirchhoff–Love Shells with Application to Wrinkling, *Computer-Aided Design* 139 (2021) 103075.
- [26] Delft High Performance Computing Centre (DHPC), DelftBlue Supercomputer (Phase 1), <https://www.tudelft.nl/dhpc/ark:/44463/DelftBluePhase1>, 2022.
- [27] B. Jüttler, U. Langer, A. Mantzaflaris, S. E. Moore, W. Zulehner, *Geometry + Simulation Modules: Implementing Isogeometric Analysis*, *PAMM* 14 (2014) 961–962.
- [28] L. Leonetti, D. Magisano, A. Madeo, G. Garcea, J. Kiendl, A. Reali, A simplified Kirchhoff–Love large deformation model for elastic shells and its effective isogeometric formulation, *Computer Methods in Applied Mechanics and Engineering* 354 (2019) 369–396.
- [29] A. J. Herrema, E. L. Johnson, D. Proserpio, M. C. Wu, J. Kiendl, M.-C. Hsu, Penalty coupling of non-matching isogeometric Kirchhoff–Love shell patches with application to composite wind turbine blades, *Computer Methods in Applied Mechanics and Engineering* 346 (2019) 810–840.
- [30] Y. Başar, M. Itskov, Finite element formulation of the Ogden material model with application to rubber-like shells, *International Journal for Numerical Methods in Engineering* (1998).
- [31] A. Pagani, E. Carrera, Unified formulation of geometrically nonlinear refined beam theories, *Mechanics of Advanced Materials and Structures* 25 (2018) 15–31.
- [32] H. M. Verhelst, M. Moller, J. Den Besten, F. Vermolen, M. Kaminski, Equilibrium Path Analysis Including Bifurcations with an Arc-Length Method Avoiding A Priori Perturbations, *Proceedings of ENUMATH2019 Conference* (2020).
- [33] M. J. Borden, T. J. Hughes, C. M. Landis, C. V. Verhoosel, A higher-order phase-field model for brittle fracture: Formulation and analysis within the isogeometric analysis framework, *Computer Methods in Applied Mechanics and Engineering* 273 (2014) 100–118.